Journal of Applied Polymer Science

Fabrication by photoinitiated polymerization and characterization of millimeter-size poly(divinyl benzene) hollow foam shells

Yi Yang,[1,2,3] Xuan Luo,[2] Zefu Li,[1,2,3] Jia Wang,[2] Zhijun Wei,[2] Xiaojun Wang,[2] Lin Zhang[1,2,3]

[1]School of Materials Science and Engineering, Southwest University of Science and Technology, Mianyang 621010, China

[2]Science and Technology on Plasma Physics Laboratory, Research Center of Laser Fusion, China Academy of Engineering Physics, Mianyang 621900, China

[3]Joint Laboratory for Extreme Conditions Matter Properties, Southwest University of Science and Technology and Research Center of Laser Fusion, China Academy of Engineering Physics (CAEP), Mianyang 621010, China

Correspondence to: L. Zhang (E-mail: zhlmy@sina.com)

ABSTRACT: In this study, millimeter-size compound droplets were prepared easily by a one-step microfluidic method. We varied the diameter and wall thickness of the shells over a wide range by setting the flow rate. Poly(divinyl benzene) (PDVB) shells with a 3–4.8 mm diameter were fabricated through photopolymerization and supercritical drying. The gel point of photopolymerization was monitored by a rotational rheometer. Moreover, the influence of the oil-soluble photoinitiator phenyl bis(2,4,6-trimethyl benzoyl) phosphine oxide (BAPO) on the properties of the foam shell were investigated by transmission electron microscopy, scanning electron microscopy, and nitrogen sorption measurements. Significant differences in the mechanical properties and porous features were obtained for different BAPO concentrations. The surface areas of the foam shells decreased, and the densities of the foam shells increased with increasing BAPO concentration. In addition, the nonconcentricity and out-of-roundness values were mainly less than 7 and 3%, respectively, for most of the shells. The results indicate that the PDVB hollow foam shells are a promising inertial fusion energy target. © 2014 Wiley Periodicals, Inc. J. Appl. Polym. Sci. **2015**, *132*, 41625.

KEYWORDS: foams; photopolymerization; porous materials; properties and characterization; rheology

Received 2 July 2014; accepted 18 October 2014

DOI: 10.1002/app.41625

INTRODUCTION

Monodisperse porous polymeric microspheres are attractive for considerable applications, including coatings, calibration standards of various instruments, chromatographic support materials, synthetic receptors, controlled drug-release vehicles, enzymes and catalysts, and inertial confinement fusion (ICF).[1–5] Compared to conventional materials, polymeric microspheres are more remarkable for their additional characteristics, including a high specific surface area, chemical stability, and low density. However, hollow foam microspheres targeted for ICF with both a low density and size uniformity are not easily fabricated. Various materials have been researched previously; these include resorcinol–formaldehyde aerogel,[6–9] trimethyl propane trimethacrylate,[10,11] and poly(divinyl benzene) (PDVB).[12,13] Among these materials, PDVB is worth investigating because it could prevent the reduction of an energy yield caused by oxygen in inertial fusion energy (IFE) experiments.[14] Furthermore, DVB, which contains divinyl, is more reactive than its monovinyl counterparts. Thus, DVB could be fully crosslinked and produced as a foam within the density range of interest and a cell size of 1–4 sμm.[12]

A variety of physical and chemical methods might be applied to prepare foam shells. Emulsion polymerization is a complicated process influenced by a number of convoluted, thermodynamic, and kinetic factors.[15] The distillation–precipitation polymerization technique involves a multistep reaction and core removal.[16] A layer-by-layer assembly technique is a better method for obtaining pure product; this is only suitable for polymer electrolytes via electrostatic interactions.[17] In general, micrometer-size spheres are facilely obtained by those methods. Recently, millimeter-size shells have begun to raise attention for their special applications in laser fusion experiments or as mandrels for ICF targets.[12,13,18,19] In particular, in IFE experiments, a higher yield energy can be obtained with millimeter-size shells. Compared with small- or medium-size shells, the size of millimeter-size shells generally ranges from 1.5–4 mm; this depends on the experiment type. To fabricate millimeter-size PDVB shells for the National Ignition Facility, a triple-orifice droplet was introduced by Streit and Schroen[12] and Paguio *et al.*[13] However, the

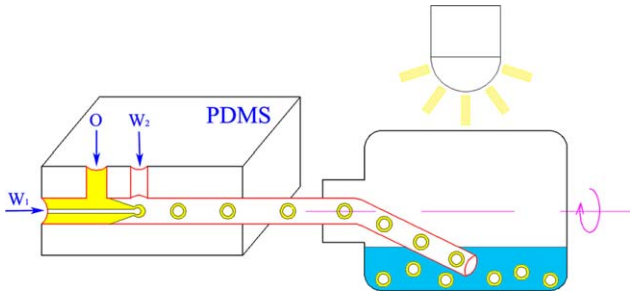

Scheme 1. Schematic illustration of the fabrication of the PDVB hollow foam shells via microfluidics and photopolymerization. [Color figure can be viewed in the online issue, which is available at wileyonlinelibrary.com.]

triple-orifice droplet generator was restricted by a higher request of assembly precision. Microfluidics could offer a convenient and finely controllable route for the synthesis of microspheres.[20–23] Moreover, during the preparation of the shell, polymerization is a major factor that could not be neglected. A density match between the inner water phase and oil (O) phase at the gelation temperature is required for traditional heat polymerization during the fabrication of a hollow microcapsule.[24] The stability of multiple-emulsion droplets decreased when the inner water phase was close to the boiling point caused by high temperatures (60–80°C). As one major technique, rapid and convenient photopolymerization at room temperature is the best choice for preventing some questions caused by heat polymerization, such as poor stability of the emulsion droplet and agglomerate. Furthermore, it is worth noting that the fabrication of millimeter-sized PDVB foam shells by photopolymerization with the microfluide technique has not yet been reported in the literature.

In this study, millimeter-size PDVB hollow shells were prepared by photopolymerization with a microfluide technique. Monodisperse double emulsions were fabricated by a coflow microfluidic chip in one step, and their size was easily varied by changes in the flow conditions. Moreover, the effects of the photoinitiator concentrations for the photopolymerization were investigated. The gel point, the main concern for the curing process, was monitored by rotational rheometer. Moreover, the density, surface area, and pores structure of the foam shells were also investigated in detail. On the basis of the previous studies, millimeter-sized PDVB hollow shells with a controllable density and pore structure were obtained.

EXPERIMENTAL

Materials

Technical-grade divinyl benzene (DVB; composed of 80% DVB and 20% ethyl vinyl benzene, Aldrich) were purified by reduced-pressure distillation to remove the inhibitors. Phenyl bis(2,4,6-trimethyl benzoyl) phosphine oxide (BAPO; purity > 97%, Aldrich) was used as a photoinitiator without further purification. The emulsifier was sorbitan monooleate (Span 80, chemical grade, hydrophile lipophilic balance (HLB) = 4.3, Tianjin Kemiou Chemical Reagent Co.). Dibutyl phthalate (analytical grade, Chengdu Union Chemical Industry Reagent Research Institute), poly(vinyl alcohol) (PVA; weight-average molecular weight = 88,000 g/mol, Acros Organic), and polydimethylsiloxane (PDMS; Dow Corning) were used as received.

Preparation of the Samples

We fabricated the microfluidic chip by pouring PDMS on a glass wafer with removable models.[25] After UV-light modification, the higher quality hydrophobic properties of the PDMS chip can be greatly improved. The schematic illustration is shown in Scheme 1. To match the density with the O phase under room temperature, the inner water phase was composed of D_2O and H_2O with a 34:100 volume ratio. BAPO and Span80 were dissolved in a mixture of the O phase composed of 20 vol % divinyl benzene and 80 vol % dibutyl phthalate. The continuous phase was an aqueous solution of 5 wt % PVA.

The internal water (W_1), O, and external water (W_2) was pushed into the microfluidic channel by motor-driven syringe pumps. With an appropriate flow rate ratio, the W_1 phase, which was delivered by a needle, could be encapsulated by the O phase at the exit. At the same time, the W_1/O emulsion was stripped off the exit under the shear forces of the continuous phase to form an O droplet filled with the water phase. The formation process of the W_1/O/W_2 was observed by a charge-coupled device camera. Argon was pushed into the flask to remove oxygen. Subsequently, the droplet was exposed to UV light (wavelength of light, $\lambda = 365$ nm, intensity of light, $I = 3.7$ W/cm^3) for polymerization. After 60–90 min, the solidified shells were put into distilled water to remove PVA and then placed in acetone to replace dibutyl phthalate and inner water

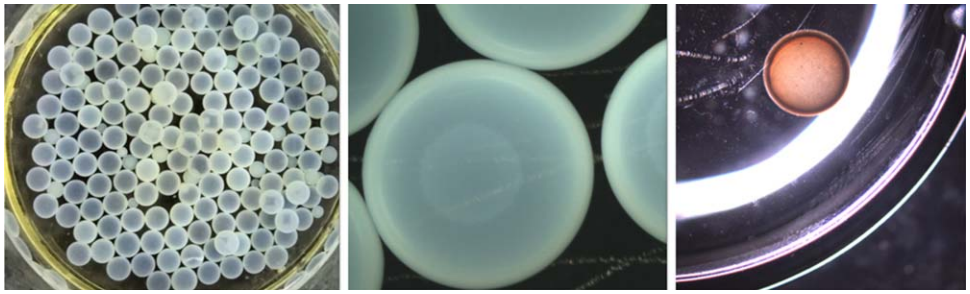

Figure 1. Hollow structures observed in solvents with different refractive indices: (A) ethanol ($n = 1.361$), (B) acetone ($n = 1.358$), and (C) chloroform ($n = 1.445$), where n is refractive index. The percentage of BAPO in the O phase was 3 wt % with respect to DVB. [Color figure can be viewed in the online issue, which is available at wileyonlinelibrary.com.]

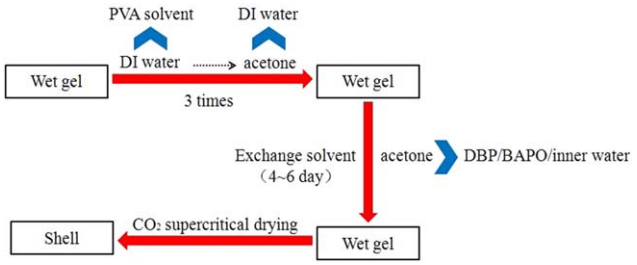

Scheme 2. Schematic diagram of the experimental process for the preparation of the shell (DI = deionized). [Color figure can be viewed in the online issue, which is available at wileyonlinelibrary.com.]

by solution exchanges for 4–6 days. The gel became transparent in an index-matching solvent. The surviving shells in solvent with different refractive indices are shown in Figure 1. The intact foam shells were then obtained by a CO_2 supercritical dryer. The schematic diagram of the preparation method is presented in Scheme 2.

Characterization of the Samples

The online viscosity was monitored with a rotational rheometer (AR550, TA) at 20°C. The hollow structure of shells was measured by X-ray radiography. The mechanical properties of shells were investigated by thermomechanical analysis (TMA; 402 F1, Netzsch). Nitrogen adsorption/desorption was measured by a Quadrasorb SI instrument. Before analysis, samples were degassed *in vacuo* at a temperature of 150°C for 24 h. The specific surface areas were determined by the Brunauer–Emmett–Teller (BET) method from nitrogen adsorption measurements at −196°C. The total pore volume is the single-point adsorption at $P/P_0 = 0.98$, where P is partial pressure of adsorbate; P_0 is saturated vapor pressure of sorbent. The section of the shells was observed with scanning electron microscopy (SEM; Ultra 55 microscope).

RESULT AND DISCUSSION

Effect of the Flow Rates on the Droplet Sizes

Multiple emulsions are often prepared by a two-step process and commonly stabilized with an amphiprotic surfactant.[24,26] Recently, some reports have shown that multiple emulsions could be also produced through a one-step method; this enabled the production of multiple emulsions with a wide range of shell thicknesses.[27] A controllable drop-in-drop structure was successfully produced in one step by the chip module shown in Scheme.1. Droplets with a uniform size were formed, and their size was easily varied by the tuning of the three fluids' flow rate. Figure 2 shows the effects of the flow rates on the size of the droplets. Although the flow rates of the constant oil phase (Q_o) and inner water phase (Q_i) were 3 and 5 mL/h, respectively, the average size of the droplet decreased with increasing flow rate of the continuous phase (Q_c) from 30 to 130 mL/h [Figure 2(A)]. This result occurred because at low Q_c (<10 mL/h), the continuous phase could not offer enough shear force for the droplets to rupture. In the case of high Q_c, where inertia begins to work, the drag force and capillary force were balanced during droplet generation. Thus, the droplet size decreased with increasing Q_c.[28,29] In addition, Q_c had a slight effect on the wall thickness of the droplets. Satellite droplets were also generated in the wake of the primary droplets.[30]

At a fixed Q_c phase (90 mL/h), the droplet size was affected by the ratio of Q_i to Q_o. Figure 2(B) shows that the wall thickness of the droplets decreased with increasing Q_i/Q_o. The wall thickness was determined by the interfacial tension force and drag force. For a fixed system, the interfacial tension force was constant. At low Q_i/Q_o, the water drop was too small to depart from the exit, whereas the O drop surrounding it was quite large.[31] It was demonstrated that the overall droplet diameter was too small to afford enough drag force. When the wall thickness increased to an appropriate number, an intact droplet was formed by the shear force. Additionally, the overall droplet diameter was affected little by the relative flow rate of Q_i to Q_o. Thus, the size of the $W_1/O/W_2$ droplet, both internal and external droplets, was manipulated by controlling flow rates of the three fluids.

Effect of the Photoinitiator Concentrations for the Photopolymerization

With the polymerization process occurring, the transparency of the PDVB shells decreased, and the shells turned white. In addition, the wall thickness of the wet gel is commonly 200–700 μm. BAPO is one of the most active photoinitiators that

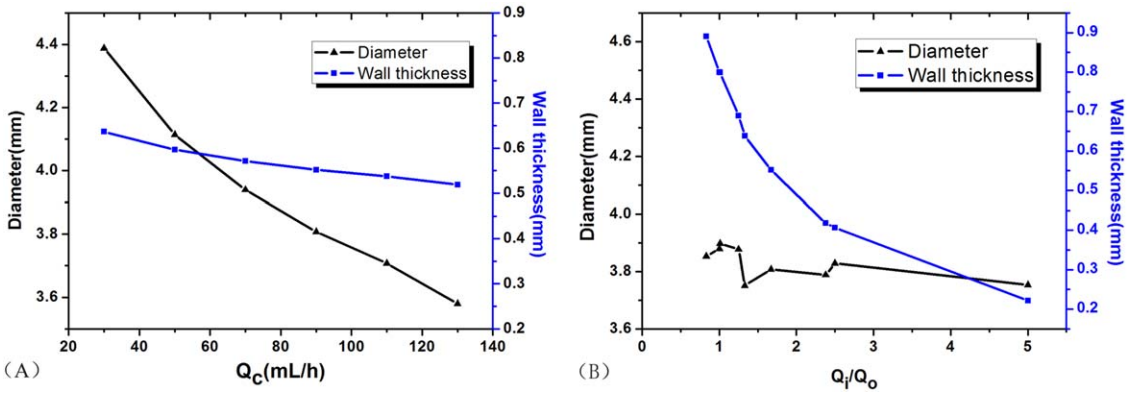

Figure 2. Effect of the flow rates on the $W_1/O/W_2$ droplet formation in one step: (A) $Q_o = 3$ mL/h and $Q_i = 5$ mL/h and (B) $Q_c = 90$ mL/h. [Color figure can be viewed in the online issue, which is available at wileyonlinelibrary.com.]

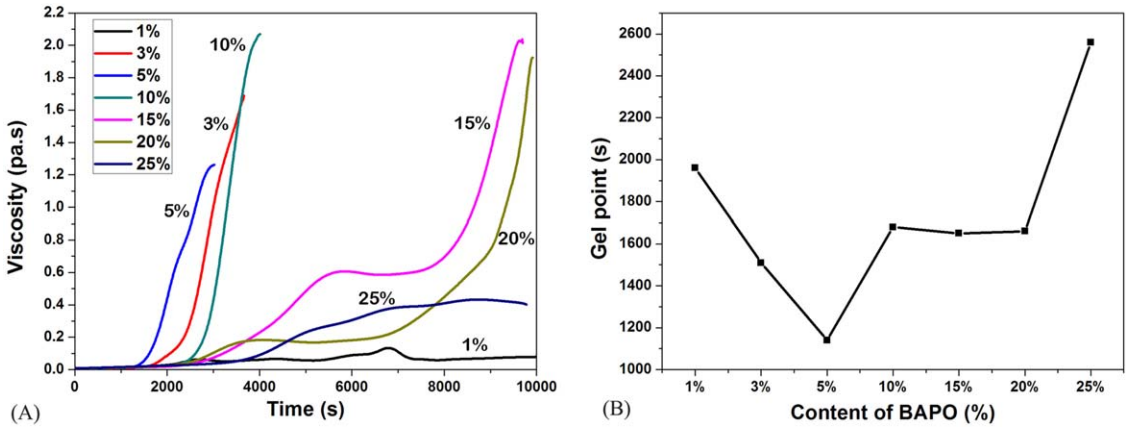

Figure 3. (A) Viscosity curves and (B) gel points for photopolymerization with different BAPO concentrations. [Color figure can be viewed in the online issue, which is available at wileyonlinelibrary.com.]

Table I. Effects of Various BAPO Contents on the Characteristics of the PDVB Shells[a]

BAPO concentration (%)[b]	D_n (mm)	T_n (mm)	σ (mm)	CV (%)	NC (%)	OOR (%)	Shrinkage (%)	Yield (%)
3	3.18	0.39	0.08	2.6	4.84	0.69	10.7	75
5	3.75	0.35	0.06	1.7	3.41	1.4	12	75
10	4.81	0.33	0.15	3.36	6.78	2.49	10.14	55
15	4.3	0.28	0.1	2.3	5.08	1.84	10.06	40
20	3.93	0.22	0.03	0.87	5.09	0.35	14.93	75
25	3.73	0.18	0.05	1.4	6.08	0.51	16.18	75

D_n, average shell diameter; T_n, average shell thickness; CV = σ/D_n.
[a] Polymerization was induced with the same intensity and wavelength of light. The theoretical density was 153 mg/cm^3.
[b] BAPO/DVB weight ratio.

belong to the phosphineoxide group.[32] Because of trimethyl benzoyl and phenyl phosphoryl, BAPO has a high efficiency and good photobleaching; this makes BAPO useful for deep-color curing. In particular, BAPO is suitable for thick-film production; it is also very important for preparing the shell. Furthermore, BAPO obviously improved the quenching of the

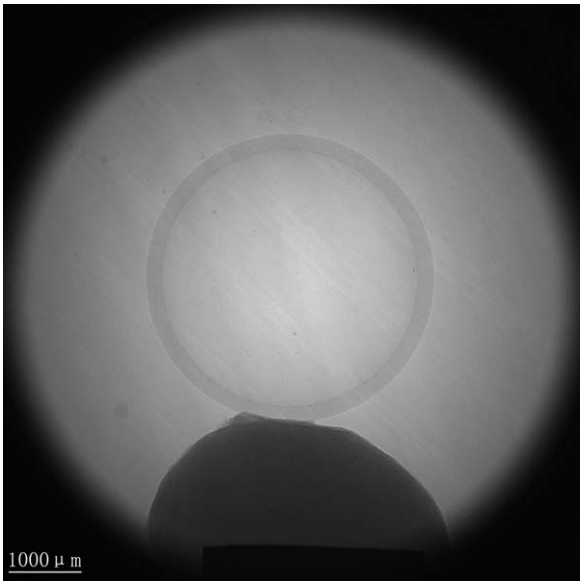

Figure 4. Hollow structure of the foam shells measured with X-ray radiography.

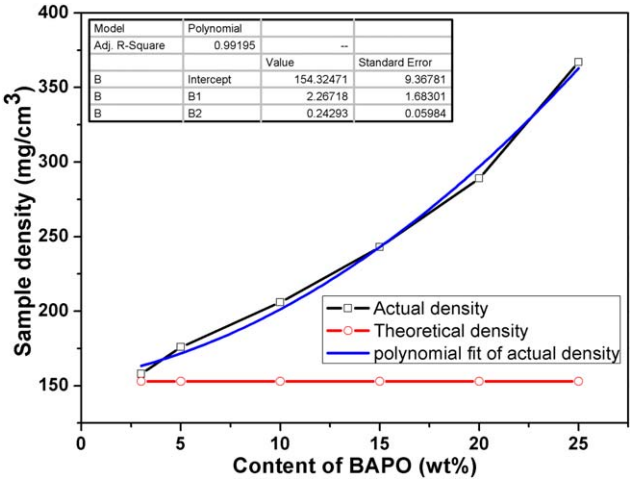

Figure 5. Sample density as a function of the BAPO concentration. [Color figure can be viewed in the online issue, which is available at wileyonlinelibrary.com.]

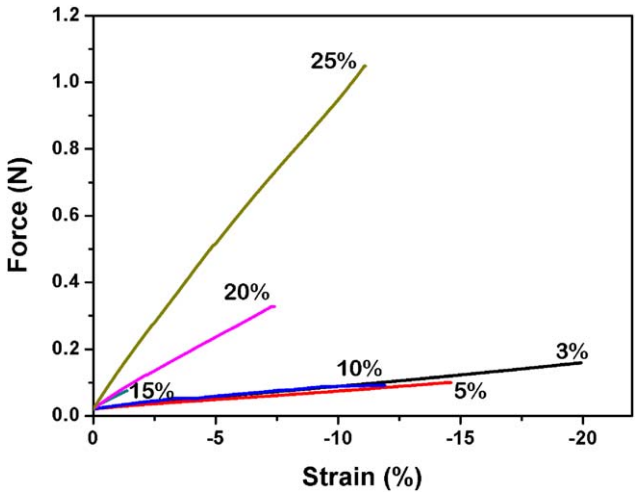

Figure 6. Compression properties of the foam shells with different BAPO concentrations. [Color figure can be viewed in the online issue, which is available at wileyonlinelibrary.com.]

free-radical DVB. Thus, it was selected to initiate the polymerization of DVB.

From the Lambert–Beer law, light will suffer from attenuation while increasing the irradiation distance. Because of the light absorption and scatter caused by additives, which brought about restricted cure on depth,[33,34] the BAPO concentration had to be limited. However, a high concentration BAPO was also required for surface curing to reduce oxygen inhibition. In addition, the concentration of the photoinitiator had a significant effect on the polymerization process and micromechanism. Therefore, the appropriate content of BAPO was meaningful.

Effect of the Photoinitiator Concentrations on the Gel Points for Photopolymerization. For the curing process, the gel point is one of the most significant characteristics. On the basis of the viscosity–time curve, the mutational site was defined as the gel point of the process. The viscosity with different concentrations of BAPO is shown in Figure 3(A). The system of the sample with 25 wt % BAPO did not full solidify until the completion of test, and only the part near the light source became hard. The solid part would not move along with the revolving armature and thus prevent the entry of UV light. Therefore, the viscosity did not drastically increase after the gel point appeared. The viscosities of the samples with 15 and 20 wt % BAPO increased to a certain extent upon the appearance of the gel point; this was caused by crosslinking near the light source. Along with the rotation of the armature, the first polymerization sample followed the rotation as well and led to a plateau phase of in the viscosity. As the illumination time increased, the whole system of samples began to crosslink, and the viscosity increased rapidly to form coagula. Samples with 3, 5, and 10 wt % BAPO showed comparatively regular changes in the viscosity. This showed a drastic increase in the viscosity when the gel point was reached; this resulted in the formation of macrogels. It indicated that the light transmittance matched the polymerization rate better and led to uniform solidification. Samples with 1 wt % BAPO, despite their minor increase in the viscosity, did not solidify, even when the illumination time was increased. After drops of the precipitating agent were added, white flocculent substances appeared, and they were thought to be microgels. The phenomenon, which the morphology of the PDVB influenced by photoinitiator concentration, was similar to that reported previously in which the morphology of PDVB as influenced by both the DVB concentration and the solvency.[35]

As shown in Figure 3(B), when the BAPO concentration increased to 5 wt %, the gel point decreased to its lowest point. There was no clear change in the gel point when the BAPO concentration was varied between 10 and 20 wt %. The gel point increased with increasing BAPO concentration. This phenomenon was similar to the characteristics of the photopolymerization.[36,37] The high concentration of initiator might have led to extinction and radical termination by coupling with each other; this was a negative factor during the polymerization progress.

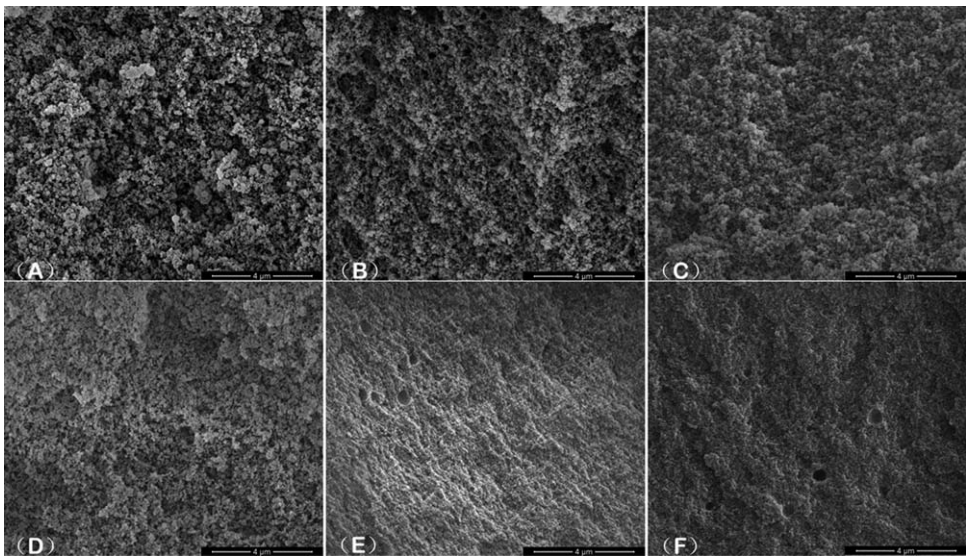

Figure 7. SEM cross sections of the foam shells with different BAPO concentrations: (A) 3, (B) 5, (C) 10, (D) 15, (E) 20, and (F) 25 wt %.

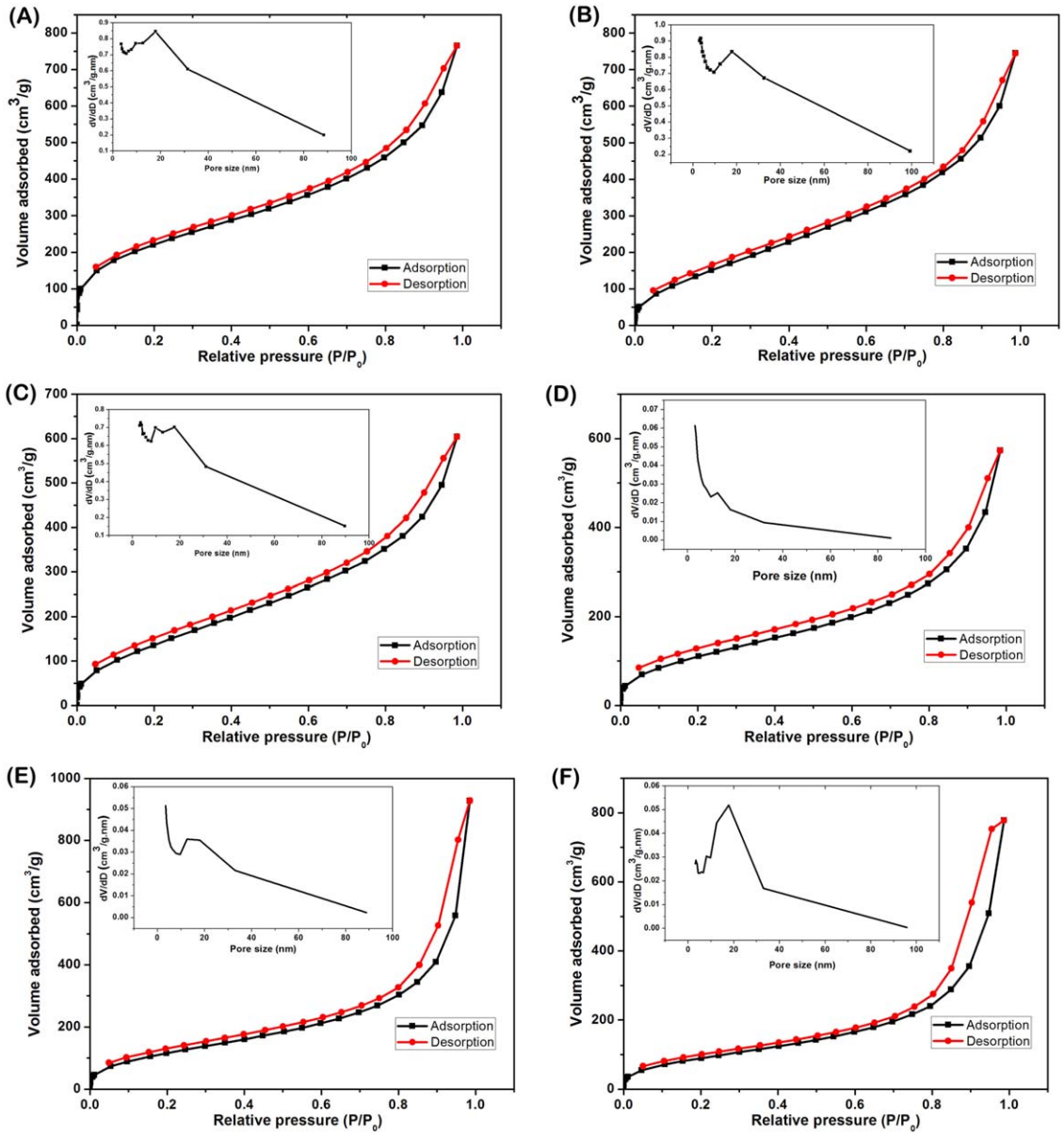

Figure 8. Isotherms of nitrogen adsorption–desorption at 77 K. The insets show the pore size distribution (upper left) of the different samples as obtained from the Barrett–Joyner–Halenda method: (A) 3, (B) 5, (C) 10, (D) 15, (E) 20, and (F) 25 wt %. [Color figure can be viewed in the online issue, which is available at wileyonlinelibrary.com.]

Table II. Porosity Characteristics of Different Samples

Sample	S_{BET} (m^2/g)	V_T (cm^3/g)	D_A (nm)
A	797.58	1.18	5.9
B	651.03	1.15	7.07
C	559.23	0.94	6.68
D	425.64	0.89	8.3
E	447.54	1.44	12.8
F	343.59	1.2	14.0

S_{BET}, surface area obtained by the BET calculation; V_T, total pore volume at the single point of adsorption at $P/P_0 = 0.98$; D_A, average pore diameter estimated by the $4V_T/A$ method.

Effect of the Photoinitiator Concentration on the Physicochemical Properties of the PDVB Shells. After washing, solution exchange, and supercritical drying, white PDVB shells were obtained. Some characteristics of the shells are shown in Table I. The diameter and wall thickness of the shells were measured by X-ray radiography (Figure 4). In the ICF experiment, larger deviations introduced asymmetry and hydrodynamic instability; they disrupted the ablation-driven implosion before a sufficient temperature and density were achieved. Therefore, the nonconcentricity (NC) of the fabricated shells was required within 5%. The out-of-roundness (OOR) could also affect NC when the inner water phase could not center the shell. NC and OOR are defined by eqs. (1) and (2):

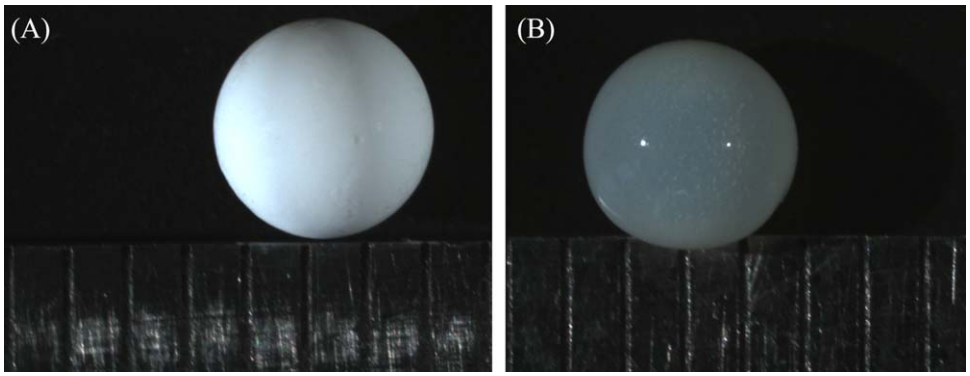

Figure 9. Optical microscopy photographs of the hollow shells with different BAPO concentrations: (A) 15 and (B) 25 wt %. The amplification factor was 6.5. [Color figure can be viewed in the online issue, which is available at wileyonlinelibrary.com.]

$$\mathrm{NC}=\frac{T_{\max}-T_{\min}}{2(\text{Average wall thickness})}\times 100\% \quad (1)$$

$$\mathrm{OOR}=\frac{D_{\max}-D_{\min}}{\text{Average diameter}}\times 100\% \quad (2)$$

where T_{max} is the maximum thickness, T_{min} is the minimum thickness, D_{max} is the maximum diameter, and D_{min} is the minimum diameter.

When the BAPO concentration is less than 15 wt %, the shrinkage of the shells was between 10 and 12%. When the BAPO concentration was higher than 15 wt %, the shrinkage increased to 16.18%. These results were formed, in part, by the bulk contraction caused by radical vinyl polymerization. On the other hand, the addition of BAPO increased the crosslinking density. In addition, the standard deviation (σ), coefficient of variation (CV), and NC reached their maxima, and OOR reached a maximum at 10 wt %. For all that, the shells with different sizes were basically monodisperse, as observed from the CV (<3.5%).

Because of the shrinkage (Table I), the actual density (ρ) was higher than the theoretical density. The final densities of the samples were found to have linear relationships with the BAPO concentrations shown in Figure 5. With polynomial fitting, the equation of the ρ and BAPO concentrations were obtained [eq. (3)]. With changing BAPO concentration, the density of the PDVB shells was adjustable under the same theoretical density:

$$\rho=0.24\chi^2+2.3\chi+154.3 \quad (3)$$

where χ is the concentration of BAPO.

The compression properties of the shells were measured by TMA (Figure 6). Under a compressive force, all of the samples were very brittle, and they shattered abruptly into granules. When the BAPO concentration increased, the total strain of the shells decreased and reached the lowest point at 15%. Thereafter, the total strain of the shells increased, and the shells were able to withstand a higher compressive force (1.05 N). The results indicate that a loose network was formed at a low BAPO concentration, and this led to a higher toughness and strain (20%). When the BAPO concentration increased, the crosslinked structure and strength of the shells was enhanced accordingly; this was caused by the increase in the active point during the polymerization process. This explained why the yield of intact shells after supercritical drying reached the lowest point when the BAPO concentration was between 10 to 15 wt %. With a further increase in the BAPO concentration (>20 wt %), a higher crosslinked structure led to an increase in the hardness, and the yield of the intact shells increased again.

Effect of the Photoinitiator Concentrations on the Pore Structures of the PDVB Shells. The SEM images of the cross section of the shells are presented in Figure 7. During the gel process, gas that dissolved in the O phase gathered gradually and formed hole structures, such as those shown in Figure 7(A–D). Because of the higher gel rate, larger pores formed at lower BAPO concentrations, and macroporous structures were observed. With increasing BAPO concentration, the pore structure became more compact. The aggregated nanoscale particles, which made up the framework structure, became smaller. According to the SEM observations, there were some pits in samples E and F. One of the possible reasons was that the gas could not run away because of the dense structure, and it formed pits after curing.

The pore properties of the samples were analyzed by nitrogen adsorption. The obtained nitrogen adsorption/desorption isotherms and pore size distribution are shown in Figure 8. The plots rise rapidly at a relative pressure of P/P_0 within the range 0.01–0.1; this indicated that there were micropores in the samples, and the adsorption at a higher relative pressure of P/P_0 indicated the presence of mesopores. Essentially, these isotherms had type IV characteristics with H4-type hysteresis loops. The H4 type of hysteresis loop is associated with capillary condensation in mesopores.[38–40] A low adsorption volume and a small loop implied a smaller pore size and lower pore volume.[41] In addition, the pore size distribution was analyzed by the Barrett–Joyner–Halenda method from the desorption branch; this revealed the polydispersion of mesopores. On this basis, Table II compares the porosity characteristics of different samples. When the BAPO concentration increased, the BET surface areas decreased from 800 to 340 m^2/g with slight increases in the total pore volume.

However, it should be noted that the appearance of the shells with different BAPO concentrations changed obviously. A disadvantage of PDVB was the opaqueness. This opacity precluded visible-light characterization; this is the current method used to characterize transparent foam and full-density shells.[15] The shells became transparent with increasing BAPO concentration

to 20–25 wt % (Figure 9). The PDVB shells with optical characteristics were comparable with transparent foam shells on some applications. With a higher BAPO concentration (>20 wt %), the shells turned pale yellow; this might have come from BAPO. To obtain colorless and transparent shells, more work will be done, such as the choice of a photoinitiator without color.

CONCLUSIONS

Monodisperse PDVB foam shells with controllable sizes were prepared by an approach that combines microfluidic and photopolymerization. The dimensional specifications of the PDVB shell ranged from 3.0 to 4.8 mm in diameter with a 180–550 μm wall thicknesses. Through the adjustment of the BAPO concentration, the density (150–370 mg/cm^3), porous structure and mechanical properties of PDVB shells could be controlled. The morphology of PDVB shells was also changed with the BAPO concentration. On the one hand, the foam shells with optimal wall uniformity and lower NC satisfied the requirement of the IFE experiments. On the other hand, the hollow shells became transparent with a high concentration of BAPO. This phenomenon might make up some applications of PDVB shells in the optics field.

ACKNOWLEDGMENTS

Financial support for this research from the Science and Technology Development Foundation of the China Academy of Engineering Physics (contract grant numbers 2012A0302015, 2012B0302050, and 2013B0302051) is gratefully acknowledged.

REFERENCES

1. Moreau, L.; Levassort, C.; Blondel, B.; De Nonancourt, C.; Croix, C.; Thibonnet, J.; Balland-Longeau, A. *Laser Part. Beams* **2009**, *27*, 537.
2. Ye, L.; Mosbach, K. *Chem. Mater.* **2008**, *20*, 859.
3. Paguio, R. R.; Frederick, C. A.; Hund, J. F.; Czechowicz, D. G.; Nikroo, A.; Takagi, M.; Acenas, O.; Thi, M. General Atomics Report. GA-A25228. October, 2005.
4. Wang, J.; Cormack, P. A. G.; Sherrington, D. C.; Khoshdel, E. *Angew. Chem. Int. Ed.* **2003**, *42*, 5336.
5. Barner, L. *Adv. Mater.* **2009**, *21*, 2547.
6. Pekala, R. W. *Mater. Sci.* **1989**, *24*, 3221.
7. Lambert, S. M.; Overturf, G. E.; Wilemski, G.; Letts, S. A.; Carey, D. S.; Cook, R. C. *Appl. Polym. Sci.* **1997**, *65*, 2111.
8. Nikroo, A.; Czechowicz, D.; Paguio, R.; Greenwood, A. L.; Takagi, M. *Fusion Technol.* **2004**, *45*, 84.
9. Meyerhofer, D. D. Presented at the 16th Target Fabrication Specialist Meeting, Scottsdale, AZ, May 3, **2005**.
10. Takagi, M.; Norimatsu, T.; Yamanaka, T.; Nakai, S. *J. Vac. Sci. Technol. A* **1991**, *9*, 820.
11. Schroen, D.; Overturf, G. E., III; Reibold, R.; Buckley, S. R.; Letts, S. A.; Cook, R. *J. Vac. Technol. A* **1995**, *13*, 2564.
12. Streit, J.; Schroen, D. *Fusion Sci. Technol.* **2003**, *43*, 321.
13. Paguio, R. R.; Nikroo, A.; Takagi, M.; Acenas, O. *J. Appl. Polym.* **2006**, *101*, 2523.
14. Sethian, J. Contract DE-AI03-94SF19892; U.S. Department of Energy: Washington, DC, **2000**.
15. Marinakos, C. J.; Bouck, K. J.; Chaput, A. B. *Macromolecules* **2000**, *33*, 1593.
16. Park, M. K.; Onishi, K.; Locklin, J.; Caruso, F.; Advincula, R. C. *Langmuir* **2003**, *19*, 8550.
17. Li, G. L.; Yang, X. L.; Bai, F. *Polymer* **2007**, *48*, 3074.
18. Chen, C.; Norimatsu, T.; Takagi, M.; Katayama, H.; Yamanaka, T.; Nakai, S. *J. Vac. Sci. Technol. A* **1991**, *9*, 340.
19. McQuillan, B. W.; Nikroo, A.; Steinman, D. A. *Fusion Technol.* **1997**, *31*, 381.
20. Dendukuri, D.; Tsoi, K.; Hatton, T. A.; Doyle, P. S. *Langmuir* **2005**, *21*, 2113.
21. Sin, D. C.; Fitzpatrick, J.; Luckman, P.; Wolvetang, E. J.; Cooper-White, J. *J. Soft Matter* **2012**, *8*, 10712.
22. Sugiura, S.; Nakajima, M.; Seki, M. *J. Am. Oil Chem. Soc.* **2002**, *79*, 515.
23. Okushima, S.; Nisisako, T.; Torii, T.; Higuchi, T. *Langmuir* **2004**, *20*, 9905.
24. Cook, R.; Takagi, M.; Mcquillan, B.; Stephens, R. The Development of Plastic Mandrels for NIF Targets. UCRL-LR-105821-00-1; Inertial Confinement Fusion (ICF) Program at Lawrence Livermore National Laboratory. October 1999 – March 2000, *1*, 1.
25. Yang, Y.; Li, Z. F.; Fang, Y.; Luo, X.; Zhang, L. *Nanotechnol. Precision Eng.* **2014**, *1*, 63.
26. Sugiura, S.; Nakajima, M.; Yamamoto, K.; Iwamoto, S.; Oda, T.; Satake, M.; Seki, M. *J. Colloid Interface Sci.* **2004**, *270*, 221.
27. Abate, A. R.; Thiele, J.; Weitz, D. A. *Lab Chip* **2011**, *11*, 253.
28. Kim, S.-H.; Shim, J. W.; Lim, J.-M.; Lee, S. Y.; Yang, S.-M. *New J. Phys.* **2009**, *11*, 075014.
29. Nunes, J. K.; Tsai, S. S. H.; Wan, J.; Stone, H. A. *J. Phys. D* **2013**, *46*, 114002.
30. Nisisako, T.; Torii, T.; Higuchi, T. *Chem. Eng. J.* **2004**, *101*, 23.
31. Shao, T.; Feng, X.; Jin, Y.; Cheng, Y. *Chem. Eng. Sci.* **2013**, *104*, 55.
32. Moon, J. H.; Shul, Y. G.; Han, H. S.; Hong, S. Y.; Choi, Y. S.; Kim, H. T. *Int. J. Adhes. Adhes.* **2005**, *25*, 301.
33. Watts, D. C. *Dent. Mater.* **2005**, *21*, 27.
34. Watts, D. C.; Amer, O.; Combe, E. *Br. Dent. J.* **1984**, *156*, 209.
35. Downey, J. S.; McIsaac, G.; Frank, R. S.; Stover, H. D. H. *Macromolecules* **2001**, *34*, 4534.
36. MeGinniss, V. D.; Provder, T.; Kac, C.; Gallopo, A. *Macromolecules* **1978**, *11*, 393.
37. Chosh, P.; Mitra, P. S.; Banariee, A. N. *J. Polym. Sci. Polym. Chem. Ed.* **1973**, *11*, 2021.
38. Zhang, L.; Chen, G.; Chen, B. W.; Liu, T. S.; Mei, Y.; Luo, X. *Mater. Lett.* **2013**, *104*, 41.
39. Huang, C. C.; Wei, Z. J.; Zhang, L.; Luo, X.; Ren, H. B.; Luo, M. M. *J. Porous Mater.* **2013**, *20*, 1017.
40. Gao, Y.; Chen, G.; We, Z. J.; Chen, B. W.; Huang, C. C.; Luo, X.; Yang, R. Z.; Bi, Y. T.; Zhang, L. *J. Sol–Gel Sci. Technol.* **2014**, *69*, 407.
41. Li, W. C.; Lu, A. H.; Schuth, F. *Chem. Mater.* **2005**, *17*, 3620.